Asian Journal of Chemistry; Vol. 32, No. 10 (2020), 2660-2670

ASIAN JOURNAL OF CHEMISTRY

https://doi.org/10.14233/ajchem.2020.22885

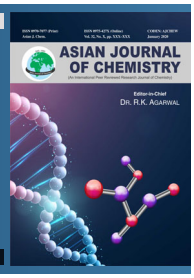

Quantum Chemical Computational Studies of Nitrogen Rich Energetic Organic Crystalline Salt: 2,4-Diamino-6-methyl-1,3,5-triazinium Trifluroacetate

K. Ayisha Begam[1,2], N.Kanagathara[2,*], R. Bhavani[3], V. Natarajan[4], B. Thirumalaiselvam[5], T. Srinivasan[6] and M.K. Marchewka[7]

[1]Department of Physics, Saveetha Engineering College, Thandalam, Chennai-602105, India
[2]Department of Physics, Saveetha School of Engineering, Saveetha Institute of Medical and Technical Sciences, Thandalam, Chennai-602105, India
[3]Department of Physics, Rajalakshmi Engineering College, Thandalam, Chennai-602105, India
[4]Department of Physics, Rajalakshmi Institute of Technology, Kuthambakkam, Chennai-602124, India
[5]Department of Physics, Vel Tech Rangarajan Dr.Sagunthala R&D Institute of Science and Technology, Chennai-600062, India
[6]Department of Physics, Agurchand Manmull Jain College, Meenambakkam, Chennai-600114
[7]Institute of Low Temperature and Structure Research, Polish Academy of Sciences, 50-950 Wroclaw, 2, P.O. Box 937, Poland

*Corresponding author: E-mail: kanagathara23275@gmail.com

Received: 4 July 2020; *Accepted*: 10 August 2020; *Published online*: 25 September 2020; AJC-20085

An organic crystalline salt 2,4-diamino-6-methyl-1,3,5-triazinium trifluroacetate (DMTFA) has been imposed for experimental and theoretical investigation. Gaussian 09 program has been used to compute the quantum chemical theoretical calculations. DFT/B3LYP-6-311++G(d,p) approach is adapted to optimize the structure. Structural and vibrational studies have been carried out by this approach followed by the correlation of experimental and theoretical results. Natural bonding orbital analysis, molecular electrostatic potential and frontier molecular orbital investigations substantiates the charge transfer besides the presence of strong inter and intra molecular interactions. Apart from the three dimensional Hirshfeld surface analysis and two dimensional fingerprint maps provides profund vision about the intermolecular interactions between the molecules.

Keywords: Triazinium trifluroacetate, Crystal structure, Hirshfeld analysis.

INTRODUCTION

Crystal engineering, the promptly flourishing versatile terrain, with ample purview for primitive research and auspicious applications. The knowledge about the framework of disparate intermolecular interaction in inorganic solids swayed the perception on supramolecular chemistry by means of non-covalent interactions [1,2]. The π-π interaction and hydrogen bonding are intermittently engaged explicit in supra molecular framework [3]. Triazine and its derivatives are inter linked array of hydrogen bonding sites, can establish explicit non-covalent supra molecular framework by the way of multiple hydrogen bonds [4]. Conjugated structures of triazine derivatives are drawing attention by virtue of its chemical flexibility and acquire prevalent applications in organic synthesis, medicinal chemistry and materials science. It is well known that organic materials with high stability and great electron infusion and transportation capacity are desirable for optoelectronic applications. Zhong *et al*. [5] prepared few new conjugated triazine based molecular materials and studied its properties for suitability in opto-electronics application.

1,3,5-Triazine derivatives are biologically active and acknowledged as anti-protozoal agents, anticancer agents, estrogen modulators, antimalarials, cyclin-dependent kinase modulator and antimicrobial agents. Further, they show applications in distinct environment, along with the manufacturing herbicides and polymer photo stabilizers. In the interest of discriminating the knowledge of systems having O-H···O and N-H···O hydrogen bonding interactions in compound, in this work, we choose 2,4-diamino-6-methyl-1,3,5-triazine (DMT) as the subject of investigation. The asymmetric unit of DMT with trichloroacetic acid was reported by Sangeetha *et al*. [6] and DMT dinitramide

was synthesized and characterized by Xiao *et al.* [7]. The presence of C-N and N-N bonds illustrates that it possess high thermal stability and density, besides the explosives, pyrotechnics and propellants which are nitrogen based materials extensively used in military. 2,4-Diamino-6-methyl-1,3,5-triazine (DMT) with various aliphatic dicarboxylic acids were studied by Xiao *et al.* [8]. Similarly, Chen *et al.* [9] examined 2,4-diamino-6-methyl-1,3,5-triazine with different salts of silver element. The existence of donor hydrogen bond and carboxylic group acceptor represents its significance in crystal engineering. The development of supramolecular structure of compounds under the array of hydrogen bond interactions are formed because of the compounds of *N*-heterocyclic group. The IR spectroscopic and quantum chemical investigation of DMT with 4-cyanobenzoic acid was studied by Mary *et al.* [10].

Perpetuo and Janczak [11] reported the structure of 2,4-diamino-6-methyl-1,3,5-triazine with trifluoroacetic acid. There are various reports available for the trifluoroacetic acid with various amino acids and other organic bases [12-18]. In continuation of findings on hydrogen bond formation in *s*-triazine derivatives in solid state, in the present study it is aimed to prepare the complex of 2,4-diamino-6-methyl-1,3,5-triazine (DMT) with trifluoroacetic acid to understand the physico-chemical properties. Thus, the experimental and theoretical studies of 2,4-diamino-6-methyl-1,3,5-triazin-1-ium trifluoroacetate (DMTFA) by using B3LYP calculations were carried out. With the guide of DFT computations utilizing B3LYP/6-311++G(d,p) basis set, vibrational frequencies, electronic properties, bonding interactions and hyperpolarizability calculations have been predicted. In extension to the above mentioned studies, Hirshfeld surface analysis has also been carried out to known in depth about the intermolecular interactions between the synthesized compound.

EXPERIMENTAL

2,4-Diamino-6-methyl-1,3,5-triazin-1-ium trifluoroacetate (DMTFA) compound was synthesized by the chemical reaction of commercially available 2,4-diamino-6-methyl-1,3,5-triazine (DMT) with 10% trifluoroacetic acid (Sd. Fine) taken in the 1:1 ratio. Solution of trifluoroacetic acid was added dropwise to the hot aqueous solution of DMT and stirred well to get a consistent solution using a magnetic stirrer. The solution was then allowed to evaporate at room temperature to yield a crystalline material salt. The solution was filtered and kept in a petri-dish. It was covered with perforated polythene cover to control the rate of evaporation. Slow evaporation of the solvent yielded many crystals (**Scheme-I**).

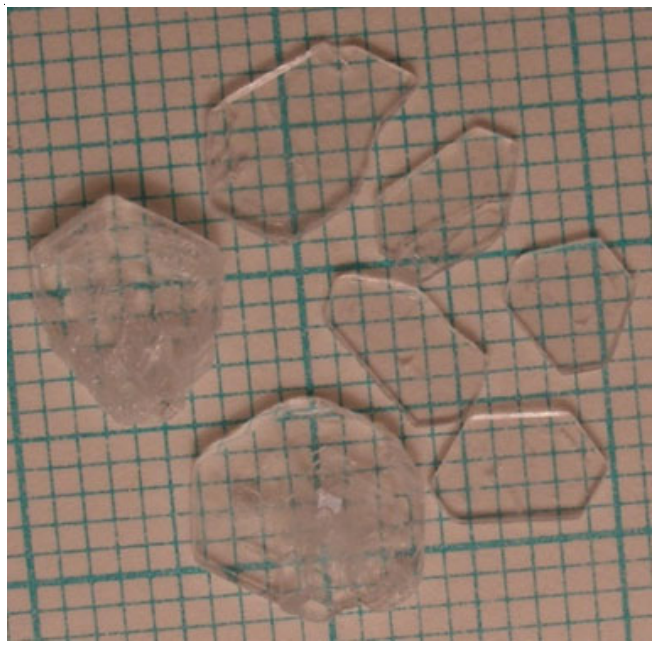

Fig. 1. Photograph of as-grown crystal of DMTFA

Quantum chemical calculations: All computations were calculated by using Gaussian 09 package with the single crystal XRD structural data as input file [19]. The optimized structure of 2,4-diamino-6-methyl-1,3,5-triazin-1-ium trifluoroacetate (DMTFA) had been obtained by the DFT/B3LYP-6-311++G (d,p) basis set. Vibrational studies has also been done with the aid of DFT approach with 6-311++G(d,p) basis set. The absence of imaginary wavenumbers on the calculated vibrational spectrum confirms the optimized structure with minimum energy. The harmonic frequencies, infrared and Raman intensities were estimated and all frequencies are scaled by 0.9665. Natural bond orbital (NBO) investigations were performed by NBO 5.1 program built in Gaussian 09 program for the equilibrium structure. Based on this result, the NBO charges and inter and intra molecular interaction between the molecules has been studied [20]. The graphic interpretation of above mentioned properties was made by Gauss View [21] program. In the case of HOMO, LUMO analysis graphic illustrations of the isosurface with value equal to 0.001 was used [21].

RESULTS AND DISCUSSION

Structural geometry: A four circle KUMA KM-4 single crystal X-ray diffractometer was used to collect the structural data of DMTFA. Single crystal XRD study reveals that the grown

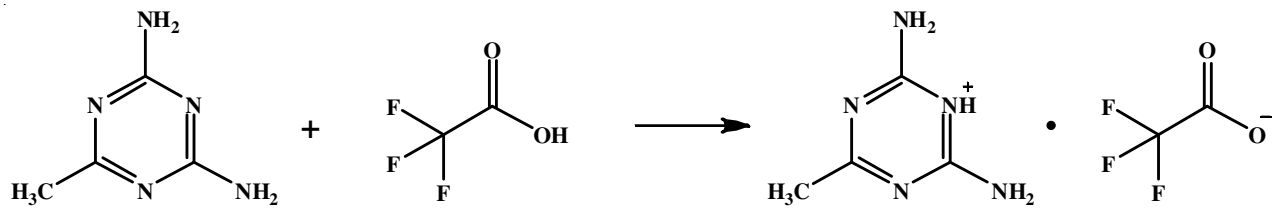

2,4-Diamino-6-methyl-1,3,5-triazine + Trifluoroacetic acid **2,4-Diamino-6-methyl-1,3,5-triazinium trifluoroacetate**

Scheme-I: Synthetic route of 2,4-diamino-6-methyl-1,3,5-triazin-1-ium trifluoroacetate (DMTFA) compound

crystal crystallizes in monoclinic system with centro symmetric space group $P2_1/c$ with primitives a = 10.384(2) Å, b = 8.1870 (10) Å, c = 13.013(3) Å and interfacial angles α = γ = 90º and β = 111.75(2)º. Fig. 2 shows the ORTEP diagram of DMTFA. The structural geometry of DMTFA attained by B3LYP/6-311++G (d,p) with atom numbering is shown in Fig. 3. DFT computed structural parameters were compared with X-ray data of reported DMTFA [11]. It is observed that the nitrogen atom (N3) in triazine ring get protonated, which has two fold crystallographic and half of the triazinium (2+) ring is independent and get hexagonal form from planar. The DFT/B3LYP calculated bond lengths of triazine ring C-N varies from 1.310 to 1.373 Å. The protonation of N5; the ring nitrogen atom lead to the decrease in C2-N5 bond length when correlated with other ring C-N bonds. The protonation leads to extension of C1-N1; C1-N2 and side chain C-NH_2 bonds. The computed internal C-N-C bond angles of C1-N2-C2 (116.19º) and C3-N1-C1 (115.79º) at the protonated N atoms are larger than the C2-N3-C3 (119.66º), which correlates well with the earlier report [11]. The variation in C-N-C angles leads to the enhancement of C1-N1 and C2-N3 bond lengths when correlated with other ring C-N bond. The internal N-C-N angle which involves in protonation *i.e*. N2-C2-N3 (120.85º) is significantly smaller than the N3-C3-N1 (121.78º) [22-24]. Due to steric effect, the lone pair electrons on the ring N atoms contributes a wider region and the internal angle is larger than that at the non-protonated ring N atoms [17,18]. The presence of disorder in CF_3 group in trifluoroacetate anion is observed [25]. The bond length of the C-F atoms are observed as C6-F1 (1.267 Å); C6-F2 (1.294 Å) and C6-F3 (1.29 Å). The mean C-F bond length is 1.2836 Å due to the results from the interaction with the neighbouring cation [26]. The N-C-N bond angles are determined by B3LYP/6-311++G (d,p) agree with the experimental values and are listed in Table-1. The CF_3COO^- ion and water molecule

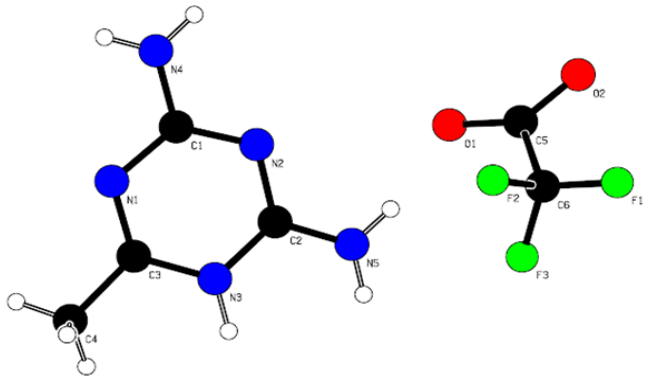

Fig. 2. ORTEP diagram of DMTFA

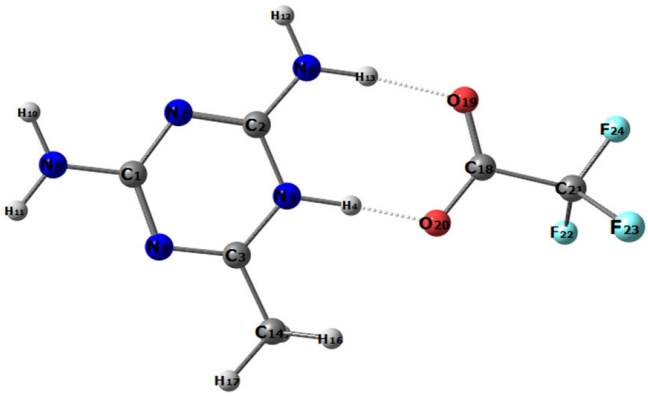

Fig. 3. Optimized structure of DMTFA

TABLE-1
SELECTED EXPERIMENTAL AND CALCULATED [B3LYP/6-311++G(d,p)] BOND DISTANCES (Å) AND BOND ANGLES (°)

Atom	Bond distance (Å)		Atom	Bond angle (°)	
	Expt.	DFT		Expt.	DFT
C1-N1	1.373	1.364	N1-C1-N2	125.53	126.309
C1-N2	1.332	1.334	C1-N2-C2	116.19	117.795
C2-N2	1.329	1.335	N2-C2-N3	120.85	120.982
C2-N3	1.362	1.372	C2-N3-C3	119.66	120.921
C2-N5	1.310	1.324	N3-C3-N1	121.78	122.485
N5-H5B	0.86	1.007	C3-N1-C1	115.79	117.374
N5-H5A	0.86	1.043	H3-N3-C2	120.16	120.861
C1-N4	1.315	1.324	H3-N3-C3	120.24	120.068
N4-H4A	0.860	1.006	C1-N4-H4A	120.00	119.353
N4-H4B	0.860	1.006	C1-N4-H4B	120.00	120.863
C3-N1	1.302	1.312	H4B-N4-H4A	120.00	121.815
C3-N3	1.356	1.352	C2-N5-H5A	120.00	121.815
C3-C4	1.484	1.495	C2-N5-H5B	120.00	120.957
C4-H4A	0.96	1.094	H5B-N5-H5A	120.00	120.957
C4-H4B	0.96	1.090	C3-C4-H4C	109.47	109.545
C4-H4C	0.96	1.088	H4B-C4-H4A	109.47	111.494
N3-H3	0.904	1.099	H4A-C4-H4C	109.47	107.761
C5-O1	1.243	1.260	H4C-C4-H4B	109.47	108.052
C5-O2	1.227	1.232	O1-C5-O2	128.43	128.778
C5-O6	1.533	1.559	C6-C5-O1	117.19	117.428
C6-F1	1.267	1.350	C6-C5-O2	114.32	113.791
C6-F2	1.294	1.353	F1-C6-F2	106.76	107.371
C6-F3	1.290	1.340	F2-C6-F3	99.69	107.471
–	–	–	F3-C6-F1	113.02	111.089

forms N-H···O and O-H···O bonds with NH_2 and NH of triazinium cations.

Vibrational band analysis: The vibrational spectra of DMTFA were computed by B3LYP with basis set 6-311++G (d,p) level. The computed values are contrasted with the observed peaks to facilitate the assignments of the peaks. Table-2 provides the theoretical and experimental values for the computed frequencies. The vibrational spectrum of the grown compound is as shown in Fig. 4, while the theoretically predicated FT-IR and FT Raman spectrum is shown in Fig. 5. The internal vibrations of the amino groups, triazine ring and trifluoroacetate anions contribute its signature in the region between 4000-400

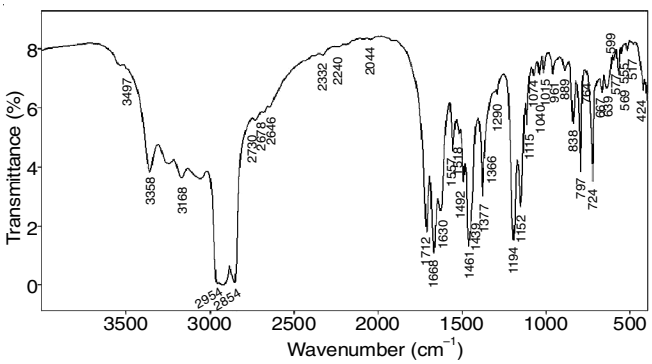

Fig. 4. FT-IR spectrum of DMTFA

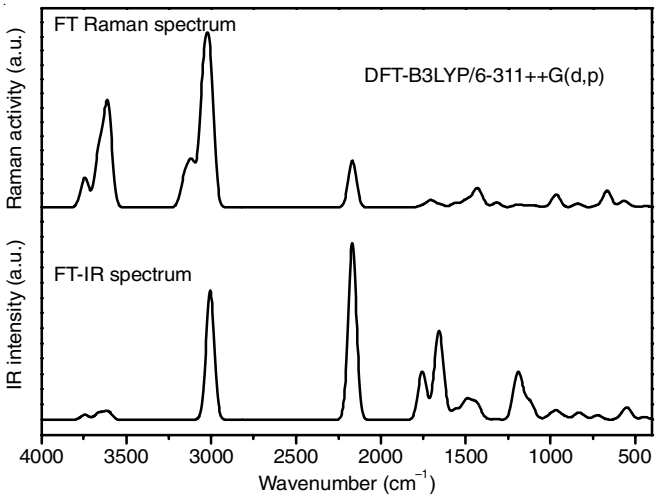

Fig. 5. Theoretical FT-IR and FT Raman spectrum of DMTFA

cm^{-1}. The lattice vibrations are observed in the Raman spectrum bands below 200 cm^{-1}.

Amino group vibrations: The symmetric stretching vibrations of the NH_2 groups are in general electron donating group and lie in the range of 3450-3250 cm^{-1} [27]. The free and interacting NH stretching vibrations of triazine cation give sharp peaks at higher wave numbers [28]. Theoretically NH_2 asymmetric stretching oscillations are calculated at 3617 and 3537

TABLE-2
WAVENUMBERS (cm^{-1}) AND RELATIVE INTENSITIES OF OBSERVED AND CALCULATED FOURIER INFRARED AND RAMAN SPECTRA OF DMTFA

Unscaled frequency	Scaled frequency	Expt. IR (cm^{-1})	IR intensity	Raman activity	Band assignment description
3743	3617		81.1206	51.8838	NH_2 asymmetric stretching
3660	3537		109.0026	94.2559	NH_2 asymmetric stretching
3609	3488	3497	134.9033	178.2596	NH_2 symmetric stretching
3155	3049	3168	0.5087	50.272	CH_2 asymmetric stretching
3112	3007		3.0716	72.1033	CH_2 symmetric stretching
3044	2942	2954	2.6376	204.5353	CH_2 symmetric stretching
3005	2904	2854	2115.254	225.1193	N-H···O stretching
2168	2095	2044	2906.357	81.7083	N-H···O stretching
1755	1697	1712	781.3971	2.7866	C-N-H asymmetric stretching
1707	1650	1668	78.0327	11.6908	NH_2 bending
1664	1608	1630	659.3197	1.0418	C-N-C/C-N stretching
1658	1603		550.4645	3.6601	NH_2/C-N/C-O-C bending vibration
1635	1581	1567	397.1842	1.0486	NH_2/COO- bending vibration
1560	1508	1518	163.7084	7.3134	NH_2/C-N-C/C-NH_2 in-plane bending vibration
1513	1462	1461	86.6736	3.4311	NH_2/C-N-C/N-H···O in-plane bending vibration
1490	1440	1439	245.6985	7.264	C-H/N-H stretching
1486	1436		14.889	3.3631	CH_2 in-plane bending
1460	1411		33.2662	2.5526	CH_3 in-plane bending
1441	1393		177.159	9.7738	C-C/COO triflouroacetic acid
1426	1378	1366	90.8526	21.9205	CH_3/C-N-C ring vibration
1397	1350	1317	23.325	5.4752	CH_3/C-N-C ring vibration
1315	1271	1290	9.6988	8.4265	C-N-C/C-NH_2/C-CH_3 bending vibration
1209	1168		23.0736	0.7365	NH_2 rocking
1199	1159	1194	550.3901	2.5921	CF_3/C-C/COO (trifluroacetic) ring vibration
1171	1132	1152	128.8561	0.7371	C-F asymmetric bending
1169	1130	1115	237.545	2.1088	CF_3 asym/C-C trifluroacetic bending
1120	1082	1074	257.3847	1.3663	CF_3 asym bending
1105	1068		6.8137	1.1574	NH_2/CH_3 in ring/C-NH_2/C-CH_3 outplane bending
1093	1056		31.6056	1.4604	CH_3/NH_3 ring distorsion
1060	1025	1015	3.9925	0.365	CH_3 out-plane bending

1008	974	961	53.9366	1.2451	C-N-C/C-CH_3/C-NH_2 bending
983	950		6.0108	0.3353	C-N/C-NH_2/C-CH_3 bending
966	933		133.3939	21.8579	N-H···O stretching/C-N stretching
917	887	889	52.7487	0.1065	N-H···O stretching
839	811	838	98.4547	6.3798	O-C-O/CF_3 asymmetric bending
808	781	797	27.8906	0.112	C-N-C/CH_3 asymmetric bending
797	770	764	17.317	0.2226	COO/CF_3 asymmetric bending
737	713	724	3.0163	0.0247	C-N bending
722	697	667	73.0145	2.7417	CF_3/COO trifluroacetic
665	643	639	4.6089	28.9217	Ring vibration
605	585	599	1.5046	0.6056	C-CH_3/C-NH_2 vibration
592	572	569	9.9914	1.3657	CF_3/COO trifluroacetic
590	571		1.1046	0.2386	NH_2 out plane bending
570	551	555	41.0006	5.6767	Ring vibration
558	540		54.5875	4.0638	Ring vibration/N-H…O stretching
546	528		0.5166	0.5969	Ring vibration/NH_2/CH_3 bending
539	521	517	132.8573	0.3389	N-H···O stretching
516	498		0.3742	0.7686	CF_3 asymm bending
451	436		30.7821	0.9675	CF_3 asym/COO bending
430	416	424	15.3337	1.2433	CF_3 asym/COO
361	349		6.0073	3.2084	NH_2 ring vibration
311	301		1.1383	0.7926	NH_2 ring vibration
294	284		207.4592	0.0153	NH_2 ring vibration
287	278		8.1665	0.0803	CF_3/COO trifluroacetic
266	257		1.852	0.9936	CF_3/COO trifluroacetic
194	187		0.9497	0.0719	C-NH_2 bending
192	185		6.1039	0.1633	C-NH_3 bending
170	164		34.2006	0.9107	Lattice vibration
167	162		19.3521	0.3503	Lattice vibration
106	102		4.9756	0.4421	Lattice vibration
77	75		2.7927	0.2978	Lattice vibration
71	69		0.1395	1.6102	Lattice vibration
60	58		0.1817	0.7599	Lattice vibration
55	53		0.0831	0.5105	Lattice vibration
26	25		0.5076	2.1603	Lattice vibration
16	16		0.0015	1.0884	Lattice vibration

cm^{-1} and symmetric stretching vibrations are at 3488 cm^{-1}. Experimentally this peak is obtained in infrared spectrum at 3497 cm^{-1} with medium intensity. Fernandez-Liencres *et al*. [29] observed this peak at 3328 cm^{-1} in 1,3,5-triazine derivatives. The intramolecular repulsive nature of amino groups results in protonation further enhanced by trifluoroacetate ion *i.e*. the distance of N-H is 0.86 Å in N-H···O interaction. A strong IR band at 1668 cm^{-1} is designated to the NH_2 bending type of vibration and theoretically this peak is detected at 1650 cm^{-1} [30]. The computed NH_2 bending type of vibration occurs at 1168, 1068 and 974 cm^{-1}. The twisting and wagging modes of NH_2 appear below 700 cm^{-1}, theoretical and experimental band at 585, 571/599 cm^{-1} is ascribed to NH_2 wagging [30].

C-N vibrations: The carbon and nitrogen bond distance in triazine ring has appreciable effect in protonation and involves in ring stretching vibrations even N-H bond distance has high frequency vibration [30-32]. The infrared bands at 1461 cm^{-1} is due to ring semicircle and C-N stretching vibration. Theoretically this peak is detected at 1462 cm^{-1}. The out-of-plane C-N-C bending vibrations in the experimental IR spectra of DFTMA appeared at 797 cm^{-1} and theoretically this peak is attained at 781 cm^{-1}. The other computed peaks of bending and ring stretching well agree with the experimentally observed as well as reported values of similar compounds [33].

Ring vibrations of triazine: The protonation causes ring vibrations in triazine ring considerably. The carbon and nitrogen stretching and exogenous carbon and nitrogen bands contracts peaks are observed at 1439 and 1461 cm^{-1}. DFT compute these peaks at 1508 and 1462 cm^{-1}. The peak obtained at 599 cm^{-1} in FT-IR is designated to the side chain in-plane C-N bend while the band at 577 cm^{-1} belongs to the side chain in-plane C-N-H bend [31]. The IR band obtained at 1056 cm^{-1} is due to the ring breathing [30].

C-F vibrations: In general halide atoms are persuaded by the adjoin atom and which results in the strong characteristic absorption bands owed to the carbon-halides. Basically, the carbon-fluorine bond is the strongest one due to its short and partial ionic nature. The three fluorine atoms connected to the same carbon atom increases the strength of the bond increases by shortening its length. The mean C-F bond distance in DMTFA is determined to be 1.27 Å. Commonly this value is 1.35 Å and contributes its signature in the range 1360-1000 cm^{-1} [34]. C-F stretching vibrations of trifluroacetic acid are recorded at 1159 and 1194 cm^{-1} by Sun *et al*. [35]. Infrared bands at 1194, 1152, 1115, 1074, 764, 667 and 569 cm^{-1} are assigned to C-F stretching vibration. DFT calculated the above mentioned corresponding peaks at 1159, 1132, 1082, 811, 781, 770, 697 and 572 cm^{-1} [36,37].

C-O and C-C vibrations: The most extensively studied oscillations in the infrared spectroscopy is the C-O mode of stretching vibration. The IR absorption of the C-O in the carboxyl group observed around 1780-1700 cm^{-1}. Experimentally this peak is obtained at 1567 cm^{-1} with medium intensity. DFT computed this peak at 1581 cm^{-1}. The stretching mode of COO^- symmetric vibration is observed in the frequency range of 1450-1300 cm^{-1}. The peak at 1393 cm^{-1} is attributed COO^- vibrations of trifluoroacetate anion. The IR absorption peaks due to deformation of COO^- are usually obtained around 780-660 cm^{-1}. Here it is noticed at 764 cm^{-1} and the peak at 961 cm^{-1} in the IR is designated to C-C stretching vibrations. The computed value for the same is observed at 950 cm^{-1} [38]. The other peaks assignment is listed in Table-2.

C-H vibrations: C-H vibrations are usually observed at higher frequencies in number in infrared spectrum. In general the prominent bands of aromatic compounds usually occurs at five regions of the infrared spectrum *viz*. 3100-3000 cm^{-1} (C-H *str*.), 2000-1700 cm^{-1} (overtones and combinations), 1650-1430 cm^{-1} (C=C *str*.), 1275-1000 cm^{-1} (in-plane C-H def.) and 900-690 cm^{-1} (out-of-plane C-H def.) [27-31]. Infrared peak at 3168 and 2954 cm^{-1} is ascribed to CH_2 asymmetric and symmetric stretching vibration, respectively. Theoretically these peaks are calculated 3049, 3007 and 2942 cm^{-1}. The C-H in-plane bending vibrations are observed at 1436 and 1411 cm^{-1} with medium intensity, while the C-H out-plane bending vibrations are obtained at 1015 and 961 cm^{-1}. Other peaks are presented in Table-2.

O-H and Hydrogen bond vibrations: The O-H group vibrations observed near the 3600-3400 cm^{-1} confirms the O-H stretching band. The stretching vibrations are commonly obtained around 3500 cm^{-1} is due to hydroxyl ions. There are many hydrogen bonds of N-H···O and O-H···F types of interactions in the title compound. Amidst of them, the O-H···O bonds have an equal bond length of 2.8 Å and shows its contribution at 3005 cm^{-1} in infrared spectrum. The identical vibration in all aspects occurred at 2954 cm^{-1} in the theoretical spectrum [28].

NBO analysis: The intra- and inter-molecular interactions among bond of the grown crystals can be effectively and efficiently studied by NBO analysis [20]. If the interaction between electron donors and acceptors is the more intensive the stabilization energy "E(2)" is large, The donating tendency is more for the electron donors than that of the electron acceptors and greater the extent of unification of the whole system. Delocalization of electron density between occupied Lewis-type (bond or lone pair) NBO orbitals and formally unoccupied (antibond or Rydgberg) non-Lewis NBO orbitals correspond to balance donor-acceptor interaction [24,26].

The second order perturbation Fock-matrix theory is applied to calculate the selected donor-acceptor interactions of the title complex and the values are as indexed in Table-3. The delocalization of electron from filled Lewis type NBO to non-Lewis type NBO results in hyper conjugation effect.

For each donor (i) and acceptor (j), the stabilization energy (E_2):

$$E_2 = \Delta E_{ij} = q_i \frac{F(i,j)2}{E_i - E_j} \quad (1)$$

TABLE-3
SECOND-ORDER PERTURBATION THEORY ANALYSIS OF THE FOCK MATRIX IN NBO BASIS CALCULATED AT B3LYP/6-31G(d.p) LEVEL

	Acceptor (j)	$E^{(2)}$ (Kj mol^{-1})	E(j)-E(i) (a.u)	F(i.j) (a.u)
Within Unit 1				
BD(2)C1-N7	BD*(2)C2-N5	48.51	0.26	0.111
BD(2)C2-N5	BD*(2)C3-N9	39.22	0.34	0.106
LP(1)N6	BD*(2)C2-N5	97.63	0.20	0.132
LP(1)N7	BD*(1)C1-N9	12.17	0.83	0.091
LP(1)N7	BD*(1)C2-N5	11.48	0.80	0.086
LP(1)N8	BD*(2)C1-N7	64.58	0.25	0.119
LP(1)N9	BD*(1)C1-N 7	11.17	0.88	0.090
LP(1)N9	BD*(1)C3-N5	12.22	0.83	0.091
BD*(2)C1-N7	BD*(2)C3-N9	158.17	0.02	0.071
BD*(2)C2-N5	BD*(2)C3-N7	101.44	0.04	0.076
BD*(2)C2-N5	BD*(2)C3-N9	40.90	0.05	0.061
From Unit 1 to Unit 2				
BD(1)H-N5	BD*(1)C18O19	0.06	1.24	0.008
BD(1)H4-N5	BD*(1)C18-O20	0.32	1.20	0.018
BD(1)N6-H13	BD*(1)C18-O19	0.09	1.26	0.010
LP(1)N6	BD*(2)C18-O19	0.06	0.29	0.004
BD*(1)H4 -N5	BD*(1)C18-O19	0.06	0.25	0.012
BD*(1)H4-N5	BD*(1)C18-O20	1.58	0.21	0.052
BD(1)N6-H13	BD*(1)C18-O19	0.09	1.26	0.010
LP(1)N6	BD*(2)C18-O19	0.06	0.29	0.004
BD*(1)H4-N5	BD*(1)C18-O19	0.06	0.25	0.012
BD*(1)H4-N5	BD*(1)C18-O20	1.58	0.21	0.052
From Unit 2 to Unit 1				
LP(2)O19	BD*(1) N6-H 13	22.30	0.69	0.113
LP(1)O20	BD*(1)H4-N5	10.30	0.94	0.090
LP(2)O20	BD*(1)H4-N5	59.75	0.69	0.183
Within Unit 2				
LP(2)O19	BD*(1)C18-O20	13.93	0.83	0.098
LP(2)O19	BD*(1)C18-C21	22.48	0.59	0.103
LP(2)O20	BD*(1)C18-C21	15.61	0.66	0.092
LP(3)O20	BD*(2)C18-O19	95.03	0.27	0.143
LP(3)F22	BD*(1)C21-F23	12.14	0.66	0.080
LP(3)F22	BD*(1)C21-F24	7.85	0.67	0.065
LP(3)F23	BD*(1)C21-F22	11.84	0.66	0.079
LP(2)F24	BD*(1)C18-C21	7.29	0..72	0.066
LP(3)F24	BD*(1)C21-F22	10.38	0.66	0.074
LP(3)F24	BD*(1)C21-F23	11.01	0.65	0.076

where q_i is the occupancy of donor orbital, E_i and E_j are energies of donating and accepting orbitals and F(i,j) is the NBO Fock matrix elements.

In the title compound, all the hydrogen atoms attached to the carbon, oxygen and nitrogen atoms carry positive charge of around 0.4e . Hydrogen atoms (4H) and (13H) which take part in protonation carry the positive charges of 0.459e and 0.447e, respectively. The carbon atom 14C and 7C, which are attached to the hydrogen atoms 15H, 16H and 17H have negative charge -0.630e whereas the carbon atom 2C attached with the nitrogen atoms 5N,6N and 7N have positive charge of 0.543e; 3C attached to the carbon atom 14C, nitrogen atoms 5N and 9N have positive charge of 0.543e.The carbon atom 21C attached with the fluorine atoms 22F,23F and 24F has a positive charge of 0.986e. The carbon atom 18C attached with the 21C, 19O and 20O bears a negative charge of 0.726e. All the nitrogen atoms are having negative charge around 0.6e; whereas the

nitrogen atom 18N attached to 1C, 10H and 11H carries a negative charge of 0.736e. All the other nitrogen and oxygen atoms present in the complex carries negative charges of around 0.6e and 0.7e, respectively. The strongest intra molecular interaction energy is found to be 158.17 kJ mol^{-1}, which is due to the electrons donated from π*(C1-N7) to π*(C3-N9) results in resonance. This shows that electron cloud can accumulate at nitrogen anion, which is further confirmed by electrostatic potential studies. The next stabilization energy is 101.44 kJ mol^{-1} is due to interaction between π*(C2-N5) and π*(C3-N7), respectively. The next stabilization energy is 59.75 kJ mol^{-1} due to strong interaction is due to high intra molecular hyper conjoining interaction of lone pair of oxygen atom O20 and anti-bonding orbital interaction of 5H*(H4-N5). The next stabilization energy 95.05 kJ mol^{-1} is due to high intramolecular hyper conjoining interaction of lone pair of oxygen atom O20 to π*(C18-O19). The stabilization energy 48.51 kJ mol^{-1} is due to high hyper conjugative π*(C2-N5) and π(C1-N7). The next stabilization energy 40.90 kJ mol^{-1} is due to interaction between π*(C2-N5) and π*(C3-N9), respectively. The next stabilization energy is 39.22 kJ mol^{-1} due to the interaction between hyper conjugative π*(C3-N9) and π(C2-N5), respectively. The stabilization is energy is around 22.30 kJ mol^{-1} is due lone pair of LP(1)O19 and anti-bonding orbital interaction 5H*(N6-H13). The stabilization is energy is around 12.14 kJ mol^{-1} is due lone pair of F22 and anti-bonding orbital interaction 5H*(C21-F23), respectively. Other data are given in Table-3. Thus, it is openly observed that N-H···O, O-H···O and N-H···N intermolecular interactions important in influencing the crystal packing and vibrational frequencies in this molecule (Fig. 6).

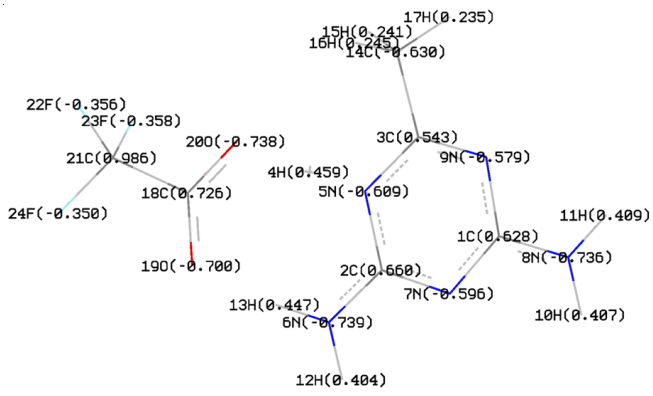

Fig. 6. NBO of DMTFA

Chemical reactivity descriptor and frontier molecular orbitals: The frontier molecular orbitals play more important role within the electric and optical properties, also as in UV-visible spectra and chemical reactions [39]. Fig. 7 shows the highest occupied molecular orbitals (HOMO) and lowest unoccupied molecular orbitals (LUMO) energy level calculated at B3LYP/6-31++G(d,p) level for the synthesized compound DMTFA. As seen from Fig. 7, both the HOMO and LUMO are localized on the DMT fragments. The p-antibonding type orbitals are mostly HOMOs and LUMOs type. The energy gap between HOMO and LUMO is the most significant parameter to determine molecular electrical transport properties. The energy

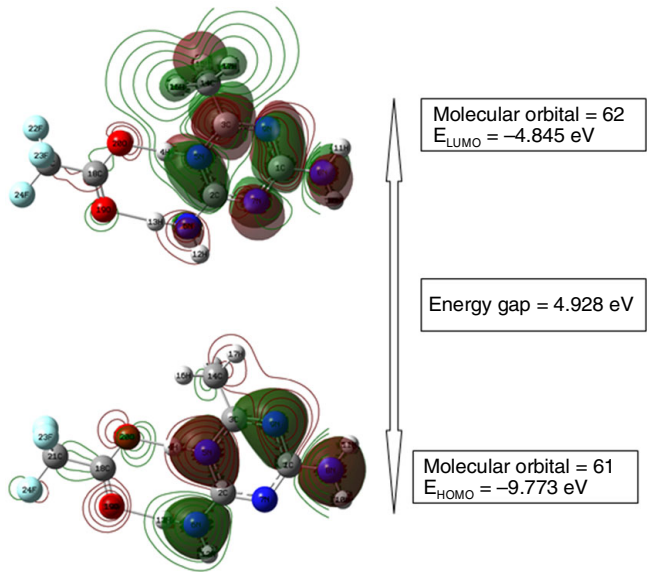

Fig. 7. HOMO-LUMO plot of DMTFA

gap is calculated to be = 4.928 eV. This large HOMO-LUMO gap means high excitation energies for many of excited states, and shows the good stability and a high chemical hardness for the title compound [40].

From HOMO and LUMO energy values for a molecule, the chemical reactivity descriptors of molecules such as hardness, chemical potential, softness, electro negativity as well as electrophilicity have been calculated [41-43]. Hardness (η), softness (S), electronegativity (χ) and chemical potential (μ) are defined follows [43]:

$$\eta = \frac{I - A}{2} \quad (1)$$

$$S = 1/2\ \eta \quad (2)$$

$$\chi = \frac{I + A}{2} \quad (3)$$

$$\mu = -\frac{I + A}{2} \quad (4)$$

where A and I are the ionization potential and electron affinity of the molecules, respectively. Through HOMO and LUMO orbital energies as $I = -E_{HOMO}$ and $A = -E_{LUMO}$ [43], one can express the ionization energy and electron affinity of the synthesized compound DMFTA. It is well known that the chemical hardness (η) and softness (S) are important properties to measure the molecular stability and reactivity. A hard molecule has a large HOMO-LUMO gap and a soft molecule has a small HOMO-LUMO gap. Soft molecules are more reactive than hard ones because they could easily offer electrons to an acceptor. For the simplest transfer of electrons, adsorption could occur at the part of the molecule where (S) has the highest magnitude whereas (η) has the lowest [44].

The chemical stability and reactivity behaviour of the title compound, the hardness, softness, electronegativity and chemical potential have been calculated and the results are presented in Table-4. To investigate the solvent effect for the chemical reactivity descriptors of the title compound, based on B3LYP/6-

311++G(d,p) model was selected and calculated values were also listed in Table-4. As seen from Table-4 that the softness decreases solvent increasing polarity, whereas hardness, electronegativity and chemical potential will increase with the increase of the solvent polarity.

TABLE-4
HOMO-LUMO ENERGY VALUE AND RELATED PROPERTIES OF DMTFA CALCULATED BY B3LYP /6-31++G(d,p) METHOD

E_{HOMO} (eV)	-9.773
E_{LUMO} (eV)	-4.845
Energy gap, ΔE (eV)	4.928
Ionization potential, A (eV)	+9.773
Electron affinity (I)	+4.845
Global softness (S)	0.203
Global hardness (η)	2.464
Chemical potential (μ)	7.309
Global electrophilicity (ω)	10.840

Electrostatic potentials: From the theoretical studies of the hydrogen bonding interactions [45,46], one can predict the electrophilic and nucleophilic reactive sites of DMTFA. The MEP of this compound has several possible sites for electrophilic attack. Negative regions were observed around the carbonyl groups of oxygen atoms due its electron affinity and establish the existence of intermolecular N-H···O, O-H···O and N-H···N non-covalent interactions in the structure [47,48].

The colour code of the maps, *i.e.* the electrostatic potential of the molecule is in the range -2.370e × 10^{-2} (deep red) to +2.370e × 10^{-2} (deep blue) where blue colour indicates the strongest attraction and red indicates the strongest repulsion. The electrostatic potentials contour map is shown in Fig. 8 . The range of total electron density of the molecule DMTFA lies in between +4.062e × 10^{-2} to -4.062e × 10^{-2} (Fig. 9).

Hirshfeld surface analysis: Hirshfeld surface investigations and 2D fingerprint plots are appropriate tools to describe the surface. The Hirshfeld surface analysis is applied to compute the intermolecular interactions of the title compound. It is an exclusive analysis for a distinct crystal structure by Crystal Explorer 3.0 [49]. Fig. 10 depicts the 100% fingerprint of DMTFA. The separations from the nearest atom inside (d_i) and outside (d_e) the surface depicts the normalized contact distance (d_{norm}). The red spots on the surface demonstrate the inter contacts made by the hydrogen atoms. The 2D Finger print plotted in

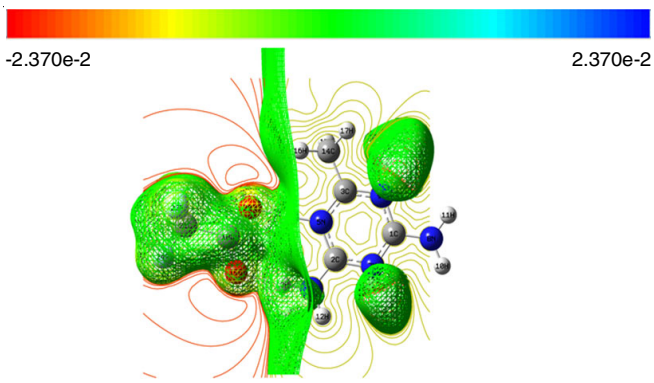

Fig. 8. Electrostatic potential map of DMTFA

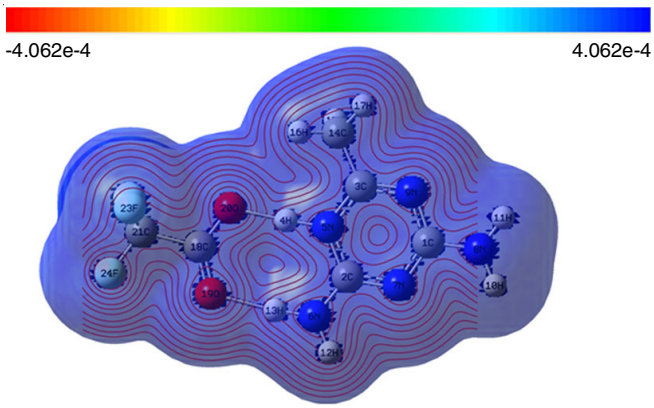

Fig. 9. Total density spectrum of DMTFA

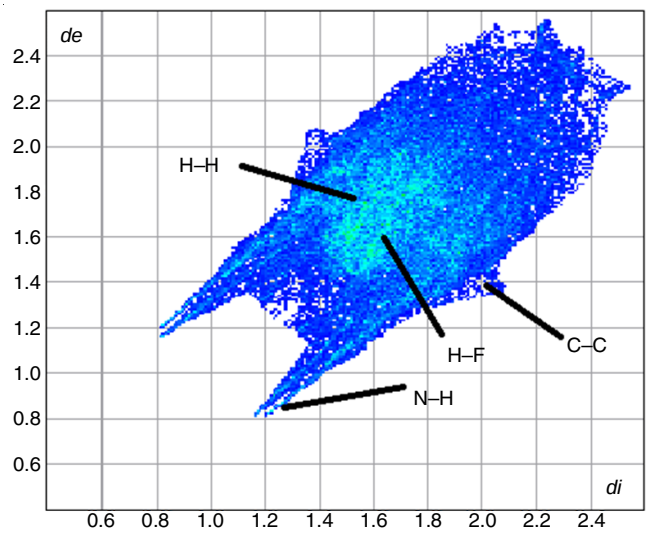

Fig. 10. Fingerprint of DMTFA (100%)

Fig. 11 depicts the inter contacts contributions. It explains that among all, the H-F interaction (26.9%) shows the major contribution. Besides H-H (16.2%), O-H (15%), N-H (14.2%), N-F (7.5%), F-F (6.5%), C-F (5.3%), C-H (3.0%), C-O (1.8%), N-O (1.7%), N-C (0.7%), O-F (0.5%) contacts also makes immense contributions to the Hirshfeld surface investigations. The inter contacts of the grown compound DMTFA is clearly seen in 3D form that have been mapped for shape index and curvature as shown in Fig. 12.

Conclusion

In this work, 2,4-diamino-6-methyl-1,3,5-triazin-1-ium trifluoroacetate (DMTFA) crystals were grown from slow solvent evaporation technique and crystallized in the centrosymmetric space group of monoclinic system ($P2_1/C$). They are theoretically optimized using B3LYP method with 6-311++G (d,p) basis set. The FT-IR vibrational spectra of DMTFA have been recorded and the computed vibrational wave numbers were calculated at B3LYP/6-311++G(d,p) basis set. The electronic structure and properties were calculated using molecular orbital analysis. The HOMO-LUMO energy gaps have been calculated to analyze the charge interaction. Besides, the NBO provide the information about the intermolecular charge transfer between the bonding and anti-bonding orbitals. An analogy between

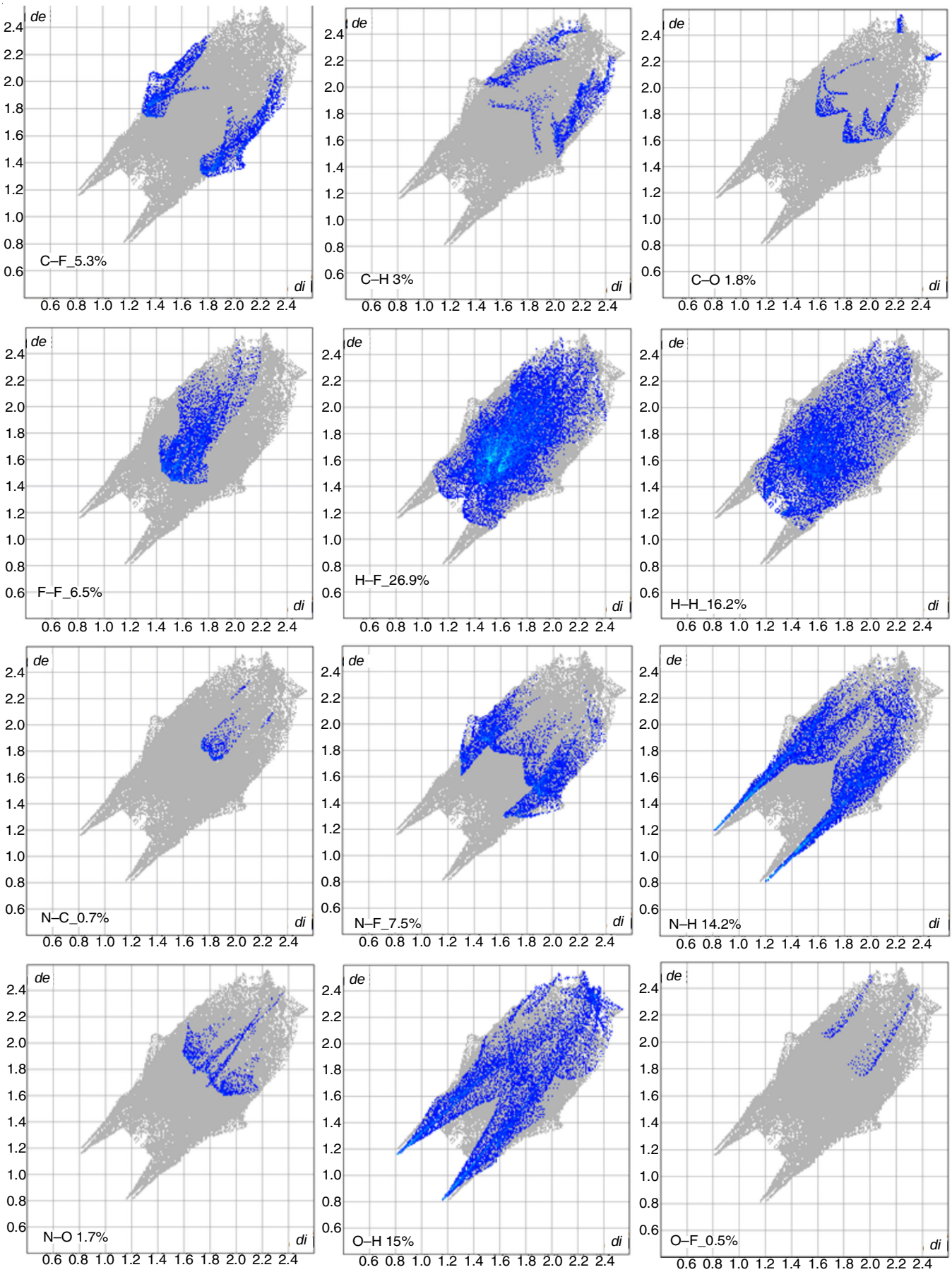

Fig. 11. Relative contributions to the percentage of Hirshfeld surface area for the various intermolecular contacts in DMTFA

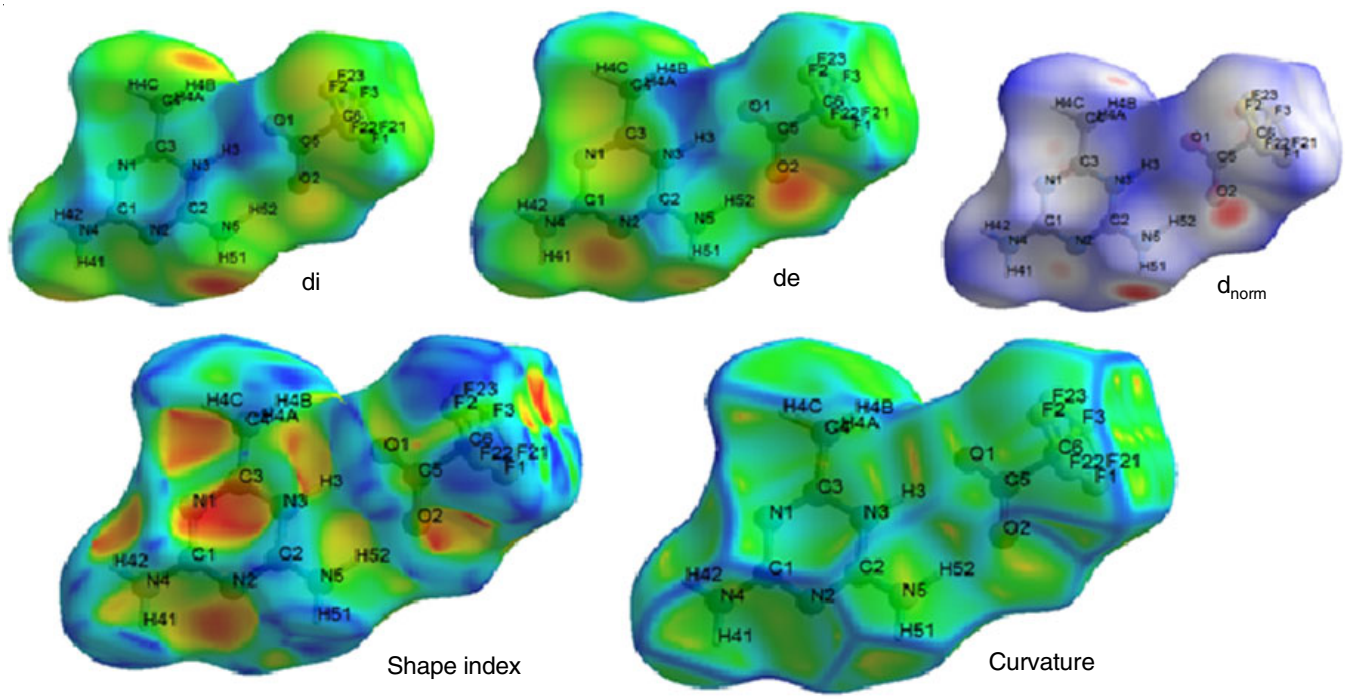

Fig. 12. Hirshfeld surface analysis di, de, d_{norm}, shape index and curvedness of DMTFA

the experimental and calculated structure reveals a good connections. Electrostatic potential map well establishes the possible nucleophilic and electrophilic reactions of the compound. The Hirshfeld surface analysis with finger plots and electrostatic potential map shed more light on the percentage of intermolecular contacts and distribution of electrostatic potential of the DMTFA compound.

CONFLICT OF INTEREST

The authors declare that there is no conflict of interests regarding the publication of this article.

REFERENCES

1. J.M. Lehn, *Pure Appl. Chem.*, **50**, 871 (1978); https://doi.org/10.1351/pac197850090871
2. J.M. Lehn, Supramolecular Chemistry, VCH: Weinheim (1995).
3. J. Barbera, L. Puig, P. Romero, J.L. Serrano and T. Sierra, *J. Am. Chem. Soc.*, **128**, 4487 (2006); https://doi.org/10.1021/ja0585477
4. G.R. Desiraju, Perspectives in Supramolecular Chemistry; The Crystal as a Supramolecular Entity, Wiley: Chichester, vol. 2 (1996).
5. H. Zhong, H. Lai and Q. Fang, *J. Phys. Chem. C*, **115**, 2423 (2011); https://doi.org/10.1021/jp109806m
6. R. Sangeetha, K. Balasubramani, K. Thanigaimani and S.J. Kavitha, *Acta Crystallogr. Sect. E Struct. Rep. Online*, **74**, 944 (2018); https://doi.org/10.1107/S2056989018008307
7. Y. Xiao, B. Jin, R. Peng, J. Zhao, Q. Liu and S. Chu, *J. Mol. Struct.*, **1146**, 417 (2017); https://doi.org/10.1016/j.molstruc.2017.06.030
8. Z.Y. Xiao, W.Q. Wang, R.Y. Xue, L. Zhao, L. Wang and Y.H. Zhang, *Sci. China Chem.*, **57**, 1731 (2014); https://doi.org/10.1007/s11426-014-5101-3
9. X.-B. Chen, S.-N. Wang, J.-F. Bai and Y.-Z. Li, *J. Coord. Chem.*, **60**, 1941 (2007); https://doi.org/10.1080/00958970601183466
10. Y. Mary, *Int. J. Ind. Chem.*, **2**, 209 (2011).
11. G.J. Perpetuo and J. Janczak, *Acta Crystallogr.*, **C63**, o271 (2007); https://doi.org/10.1107/S0108270107010165
12. D. Xu, X.Q. Wang, W.T. Yu, S.X. Xu and G.H. Zhang, *J. Cryst. Growth*, **253**, 481 (2003); https://doi.org/10.1016/S0022-0248(03)01084-4
13. N. Fuson, M.L. Josien, E.A. Jones and J.R. Lawson, *J. Chem. Phys.*, **20**, 1627 (1952); https://doi.org/10.1063/1.1700229
14. R.E. Kagarise, *J. Chem. Phys.*, **27**, 519 (1957); https://doi.org/10.1063/1.1743760
15. R.L. Redington and K.C. Lin, *Spectrochim. Acta A Mol. Biomol. Spectrosc.*, **27**, 2445 (1971); https://doi.org/10.1016/0584-8539(71)80143-5
16. R.L. Redington and K.C. Lin, *J. Chem. Phys.*, **54**, 4111 (1971); https://doi.org/10.1063/1.1675474
17. N. Singh and B. Kumar, *Physica B*, **406**, 2152 (2011); https://doi.org/10.1016/j.physb.2011.03.020
18. P.V. Dhanaraj, N.P. Rajesh, J.K. Sundar, S. Natarajan and G. Vinitha, *Mater. Chem. Phys.*, **129**, 457 (2011); https://doi.org/10.1016/j.matchemphys.2011.04.041
19. M.J. Frisch, G.W. Trucks, H.B. Schlegel, G.E. Scuseria, M.A. Robb, J.R. Cheeseman, G. Scalmani, V. Barone, B. Mennucci, G.A. Petersson, H. Nakatsuji, M. Caricato, X. Li, H.P. Hratchian, A.F. Izmaylov, J. Bloino, G. Zheng, J.L. Sonnenberg, M. Hada, M. Ehara, K. Toyota, R. Fukuda, J. Hasegawa, M. Ishida, T. Nakajima, Y. Honda, O. Kitao, H. Nakai, T. Vreven, J.A. Montgomery Jr., J.E. Peralta, F. Ogliaro, M. Bearpark, J.J. Heyd, E. Brothers, K.N. Kudin, V.N. Staroverov, R. Kobayashi, J. Normand, K. Raghavachari, A. Rendell, J.C. Burant, S.S. Iyengar, J. Tomasi, M. Cossi, N. Rega, J.M. Millam, M. Klene, J.E. Knox, J.B. Cross, V. Bakken, C. Adamo, J. Jaramillo, R. Gomperts, R.E. Stratmann, O. Yazyev, A.J. Austin, R. Cammi, C. Pomelli, J.W. Ochterski, R.L. Martin, K. Morokuma, V.G. Zakrzewski, G.A. Voth, P. Salvador, J.J. Dannenberg, S. Dapprich, A.D. Daniels, O. Farkas, J.B. Foresman, J.V. Ortiz, J. Cioslowski and D.J. Fox, Gaussian, Inc., Wallingford CT (2009).
20. F. Weinhold and E.D. Glendening, NBO Version 3.1, TCI, Madison: University of Wisconsin, Wisconsin, USA (1998).
21. R. Dennington, T. Keith and J. Millam, Semichem Inc., Shawnee Mission KS, Gauss View, Version 5 (2009).
22. R.J. Gillespie, *J. Chem. Educ.*, **40**, 295 (1963); https://doi.org/10.1021/ed040p295

23. R.J. Gillespie, *Chem. Soc. Rev.*, **21**, 59 (1992); https://doi.org/10.1039/cs9922100059
24. N. Kanagathara, M.K. Marchewka, M. Drozd, N.G. Renganathan, S. Gunasekaran and G. Anbalagan, *Spectrochim. Acta A Mol. Biomol. Spectrosc.*, **112**, 343 (2013); https://doi.org/10.1016/j.saa.2013.04.001
25. K. Aoki, M. Inaba, S. Teratani, H. Yamazaki and Y. Miyashita, *Inorg. Chem.*, **33**, 3018 (1994); https://doi.org/10.1021/ic00091a050
26. V. Sangeetha, M. Govindarajan, N. Kanagathara, M.K. Marchewka, S. Gunasekaran and G. Anbalagan, *Spectrochim. Acta A Mol. Biomol. Spectrosc.*, **125**, 252 (2014); https://doi.org/10.1016/j.saa.2014.01.018
27. N.B. Colthup, L.H. Daly and S.E. Wiberley, Introduction to Infrared and Raman Spectroscopy, Academic Press: New York (1990).
28. R.J. Meier, J.R. Maple, M.J. Hwang and A.T. Hagler, *J. Phys. Chem.*, **99**, 5445 (1995); https://doi.org/10.1021/j100015a030
29. M.P. Fernandez-Liencres, A. Navarro, J.J. Lopez-Gonzalez, M. Fernández-Gómez, J. Tomkinson and G.J. Kearley, *Chem. Phys.*, **266**, 1 (2001); https://doi.org/10.1016/S0301-0104(01)00326-3
30. W.J. Jones and W.J. Orville-Thomas, *Trans. Faraday Soc.*, **55**, 193 (1959); https://doi.org/10.1039/tf9595500193
31. P.J. Larkin, M.P. Makowski, N.B. Colthup and L.A. Flood, *Vib. Spectrosc.*, **17**, 53 (1998); https://doi.org/10.1016/S0924-2031(98)00015-0
32. Y.L. Wang, A.M. Mebel, C.J. Wu, Y.T. Chen, C.-E. Lin and J.-C. Jiang, *Faraday Trans.*, **93**, 3445 (1997); https://doi.org/10.1039/a701732d
33. M. Drozd and M.K. Marchewka, *J. Mol. Struct. THEOCHEM*, **716**, 175 (2005); https://doi.org/10.1016/j.theochem.2004.11.020
34. G. Socrates, Infrared Characteristic Group Frequencies, Wiley Intersciences Publication: New York (1980).
35. Z.H. Sun, L. Zhang, D. Xu, X.Q. Wang, X.J. Liu and G.H. Zhang, *Spectrochim. Acta A Mol. Biomol. Spectrosc.*, **71**, 663 (2008); https://doi.org/10.1016/j.saa.2008.01.024
36. M.E.D. Lestard, M.E. Tuttolomondo, D.A. Wann, H.E. Robertson, D.W.H. Rankin and A. Ben Altabef, *J. Chem. Phys.*, **131**, 214303 (2009); https://doi.org/10.1063/1.3267633
37. R.E. Robinson and R.C. Taylor, *Spectrochim. Acta*, **18**, 1093 (1962); https://doi.org/10.1016/0371-1951(62)80120-9
38. G.H. Sun, X.T. Sun, Z.H. Sun, X.Q. Wang, X.J. Liu, G.H. Zhang and D. Xu, *Growth*, **311**, 3904 (2009); https://doi.org/10.1016/j.jcrysgro.2009.06.022
39. I. Fleming, Frontier Orbitals and Organic Chemical Reactions, Wiley: London (1976).
40. H. Tanak, *J. Mol. Struct. THEOCHEM*, **950**, 5 (2010); https://doi.org/10.1016/j.theochem.2010.03.015
41. R.G. Parr, L. Szentpaly and S. Liu, *J. Am. Chem. Soc.*, **121**, 1922 (1999); https://doi.org/10.1021/ja983494x
42. P.K. Chattaraj, B. Maiti and U. Sarkar, *J. Phys. Chem. A*, **107**, 4973 (2003); https://doi.org/10.1021/jp034707u
43. R.G. Parr, R.A. Donnelly, M. Levy and W.E. Palke, *J. Chem. Phys.*, **68**, 3801 (1978); https://doi.org/10.1063/1.436185
44. N. Balamurugan, C. Charanya, S. SampathKrishnan and S. Muthu, *Spectrochim. Acta A Mol. Biomol. Spectrosc.*, **137**, 1374 (2015); https://doi.org/10.1016/j.saa.2014.09.048
45. H. Tanak, M.K. Marchewka and M. Drozd, *Spectrochim. Acta A Mol. Biomol. Spectrosc.*, **105**, 156 (2013); https://doi.org/10.1016/j.saa.2012.12.025
46. E. Scrocco and J. Tomasi, *Adv. Quantum Chem.*, **11**, 115 (1978); https://doi.org/10.1016/S0065-3276(08)60236-1
47. J. George, J.C. Prasana, S. Muthu, T.K. Kuruvilla and R.S. Saji, *Chem. Data Collect.*, **26**, 100360 (2020); https://doi.org/10.1016/j.cdc.2020.100360
48. M.H. Rahuman, S. Muthu, B. Raajaraman and M. Raja, *Chem. Data Collect.*, **26**, 100352 (2020); https://doi.org/10.1016/j.cdc.2020.100352
49. S.K. Wolff, D.J. Greenwood, J.J. McKinnon, M.J. Turner, D. Jayatilaka and M.A. Spackman, Crystal Explorer, Version 3.1 (2012).